Available online at www.sciencedirect.com
SCIENCE DIRECT®

Journal of the European Ceramic Society 23 (2003) 3059–3070

www.elsevier.com/locate/jeurceramsoc

Accommodation of impurities in α-Al_2O_3, α-Cr_2O_3 and α-Fe_2O_3

K.J.W. Atkinson[a,b], Robin W. Grimes[a,c,*], Mark R. Levy[a], Zoe L. Coull[a], Tim English[d]

[a]*Department of Materials, Imperial College, London SW7 2BP, UK*
[b]*The Royal Institution, 21 Albermarle St., London W1X 4BS, UK*
[c]*Los Alamos National Laboratory, Los Alamos, NM 87545, USA*
[d]*Corus UK Ltd, Swinden Technology Centre, Moorgate Road, Rotherham S60 3AR, UK*

Received 12 January 2002; received in revised form 28 January 2003; accepted 1 February 2003

Abstract

Atomic scale computer simulation was used to predict the mechanisms and energies associated with the accommodation of aliovalent and isovalent dopants in three host oxides with the corundum structure. Here we consider a much more extensive range of dopant ions than has previously been the case. This enables a rigorous comparison of calculated mechanism energetics. From this we predict that divalent ions are charge compensated by oxygen vacancies and tetravalent ions by cation vacancies over the full range of dopant radii. When defect associations are included in the model these conclusions remain valid. At equilibrium, defects resulting from extrinsic dopant solution dominate intrinsic processes, except for the largest dopant cations. Solution reaction energies increase markedly with increasing dopant radius. The behaviour of cluster binding energies is more complex.

Keywords: Al_2O_3; Cr_2O_3; Detect chemistry; Dopants; Fe_2O_3; Impurities; Simulations

1. Introduction

In all environments the surface chemistry of a metal will be controlled by its oxide. This is particularly pertinent for industrial processes when materials must perform at high temperatures and in highly corrosive environments where failure cannot be tolerated. In the case of aluminium, a passive α-Al_2O_3, corundum, film forms which exhibits strong bonding with the surface and imparts good corrosion resistance.[1] Stainless steel forms an oxide surface with a structure which is still debated but undoubtedly provides effective protection.[2] In the case of iron and low chromium steels various iron oxides form but impart at best only modest corrosion protection.[3]

We consider the case where these metals all form a cohesive oxide of the corundum structure. In addition to aluminium alloys this is ultimately the case in many Fe–Cr alloys in the absence of water at high temperature. However, a continuous Cr_2O_3 scale is only formed when the Cr content is above 18 wt.%.[4] Below this Cr content the scale contains iron oxides that include α-Fe_2O_3,[5] as is the case in iron and low chromium steels.[6]

In reality the structures of passive oxide films are clearly complex. While at this juncture it is not possible to model them explicitly, we seek to provide under-lying data on the corresponding bulk oxides. In particular we go beyond previous atomistic simulation studies by investigating an extensive range of dopants in three isostructural materials using a single internally consistent potential set. Thus, using computer simulation, solution mechanisms and relative equilibrium concentrations for possible alloy additions into the perfect lattices of α-Al_2O_3, α-Cr_2O_3, and α-Fe_2O_3 are predicted. These data allow us to understand qualitatively the relative importance of different impurity additions on the formation of those ionic defects (vacancies or interstitials) which, in a passive layer, could be responsible for ion transport and second phase formation. Furthermore, we will predict which impurity ions, at their equilibrium concentrations, will generate more vacancies or interstitial ions than the corresponding intrinsic reactions.

* Corresponding author. Tel.: +44-207-594-6730; fax: +44-207-584-3194.
E-mail address: r.grimes@ic.ac.uk (R.W. Grimes).

0955-2219/03/$ - see front matter © 2003 Elsevier Ltd. All rights reserved.
doi:10.1016/S0955-2219(03)00101-8

Since impurities will be present via diffusion or film growth from the underlying alloy which is being protected, it is vital to understand how important such defect impurities are to the passive surface and, in particular, to compare and contrast the effects for these three bulk oxides. This work then forms the basis from which more complete systems will be modelled in the future. Such studies may include, for example, grain boundary structures which are known to influence the resistance of stainless steels to intergranular corrosion and 'end grain' attack.[7] Furthermore redox of host cations (particularly $Fe^{3+} \rightarrow Fe^{2+}$) and the intrinsic electronic defects could also be included.

2. Defects and transport in corundum oxides

The significance of the defect and transport properties of surface oxides to the corrosion resistance of alloys has been widely recognised in the literature,[6,8–13] with much of the older work reviewed by Kofstad.[14] In addition, aluminium, chromium and iron oxides have attracted attention in their own right. Several computational studies have also been conducted in this area,[15–21] some of which have considered impurity defects. Here we comprehensively extend such work by modelling the behaviour of a very wide range of possible dopant cation species (for the time being we have not considered Cl^- or S^{2-} ions, although these could eventually also be modelled). Since modelling studies ideally complement experimental work, we will first briefly review the literature.

2.1. Defects and transport in α-Al_2O_3

Even in quite recent studies the defect chemistry of α-Al_2O_3 has not been resolved. Although it is thought to have negligible nonstoichiometry.[14] Experimental and theoretical studies concerning the dominant intrinsic disorder are found to be inconclusive.[15,16,22,23] Where a preference is stated it is for Schottky disorder[17,24] but usually only by a small margin. All studies agree however that the cation Frenkel process is of sufficiently high energy as not to play an important role. Thus, it seems impractical to differentiate between Schottky and anion Frenkel processes and it is likely that the conclusion of El-Aiat and Kröger,[22] which states that it is not possible to differentiate, categorically, between these mechanisms, is probably valid.

Studies of oxygen self-diffusion[25–27] as well as aluminium self-diffusion[8–10] show that Al is the more mobile species. Aluminium ions are thought to diffuse via a vacancy mechanism. The effect of dopants has also been studied with respect to their effect on oxygen self-diffusion. Crawley et al.[25] maintain that there is no dopant effect but Lagerlöf et al.[28,29] and Haneda et al.[30] find that magnesium doping increases the diffusion rate while titanium doping decreases it. Interestingly Perot-Ervas et al.[8] claim that, at high p_{O_2}, titanium doping is compensated by the formation of aluminium vacancies, in agreement with previous studies by Mohapatra and Kröoger[31] and Rassmussen and Kingery.[32] The charge compensating defect accompanying solution of Mg^{2+} is less clear with both oxygen vacancies and aluminium interstitials having been considered by some[33] but only oxygen vacancies by others.[30] The possibility of magnesium interstitial compensation has been proposed from modelling studies.[16]

2.2. Defects and transport in α-Cr_2O_3

Crawford and Vest[34] suggest that α-Cr_2O_3 is an intrinsic electronic conductor at high temperatures and a structural defect controlled conductor at low temperatures. α-Cr_2O_3 is not thought to exhibit any great nonstoichiometry although experiments have proved difficult. The atomistic simulation study of Lawrence et al.[19] predicts that either Schottky or anion Frenkel disorder dominates, de-pending on whether they use an empirical or non-empirical potential set.

While it seems that Cr is the mobile species[11,34,35] the mechanism is disputed (compare Ref. 35 with 11). Interestingly Hagel and Seybolt[12] determined that doping of α-Cr_2O_3 with CeO_2 or Y_2O_3 has very little effect on cation dif-fusion rates. While Y^{3+} is an isovalent dopant Ce^{4+} ions would require charge compensation in a α-Cr_2O_3 lattice. On the other hand it may be that in α-Cr_2O_3 the cerium ion assumes a 3+ charge state.

2.3. Defects and transport in α-Fe_2O_3

It is generally accepted that α-Fe_2O_3 is an intrinsic-semiconductor at high temperature[36, 37] however it also exhibits nonstoichiometry associated with oxygen vacancy formation.[38]

As with all oxides the dominant defect type depends upon pO_2 and temperature. For example, at high temperature Hoshino and Peterson[39] initially report lattice defects to be more important than intrinsic electronic defects, however, they later changed their conclusions[40] in line with Chang and Wagner,[37] who found that intrinsic electronic defects dominate.

It is reported that the diffusivity of cations decreases with increasing p_{O_2},[37,40] which leads to the conclusion that cation interstitial diffusion is responsible for lattice transport.[13,14,37,39,40] The charge state of the migrating species is debatable since it has been suggested that the interstitial ion migrates as $Fe_i^{\bullet\bullet}$ in preference to $Fe_i^{\bullet\bullet\bullet}$[39,40] although, presumably, this must depend on the extent of nonstoichiometry. There also appears to be great variation in the absolute values of diffusivity and activation enthalpy for self-diffusion[37,40] although

Atkinson and Taylor[13] have applied corrections to published data, achieving good agreement across several types of experimental methodology. Some workers comment on variations in results between samples thought to be due to different impurity concentrations.[39,40]

Although the review of the literature presented here is brief, it is clear that these three isostructural oxides present remarkably complex defect chemistries. Our aim is therefore to provide a set of defect energies for our dopant cations that predict how the solution mechanisms will change as a function of dopant cation radius. We hope such general trends, rather than absolute energies, will be particularly amenable to experimental investigation.

3. Simulation methodology

3.1. Ionic interactions

The simulations employ the Born model of ionic solids to represent interactions between ions.[41,42] Both long range coulombic forces and short range interactions are included. Thus the energy, E_{ij}, for the interaction between two ions i and j has the form,

$$E_{ij} = \frac{q_i q_j}{4\pi\varepsilon_0 r_{ij}} + A_{ij}\exp\left(\frac{-r_{ij}}{\rho_{ij}}\right) - \frac{C_{ij}}{r_{ij}^6} \quad (1)$$

where q is the charge on the ion, r_{ij} is the ion separation, and A, ρ, and C are parametrized variables specific to the interaction of ions i and j. Ionic polarisability is included by employing a shell model for oxygen ions.[43] The shell charge for oxygen was $-2.04\ |e|$ and the spring constant was 6.3 eV Å^{-2}.

3.2. Lattice simulations

The host perfect lattice is simulated by assigning ions to a unit cell that is repeated throughout space using periodic boundary conditions. The total energy of the lattice is minimised by allowing the ions in the unit cell and the lattice vectors to relax to zero strain. This is known as a constant pressure calculation. The model is verified by comparing predicted and experimental lattice parameters. The short range parameters (A, ρ, and C) are adjusted to give good agreement with experimental data. The potentials used in this study were derived or taken from the literature as indicated in Table 1.

3.3. Defect simulations

Once the perfect lattice has been established, defects are introduced around one site in the lattice. Adjacent or coincident to this point a centre is chosen and two spherical regions are defined. Region I extends from the centre to some predetermined radius. Within region I interactions are calculated explicitly and all ions are relaxed to zero force. Region II extends from the edge of region I to infinity. Region II is further sub-divided into region IIa and IIb, where the inner IIa acts as a transition between regions I and II. In IIa ion displacements are calculated by using the Mott-Littleton approximation,[44] but interactions with ions in region I are calculated by explicit summation. The contribution to the total defect energy from ions in region IIb is calculated using only the Mott–Littleton approximation. The radii of regions I and IIa have a direct impact on the accuracy of the calculated defect energy and also the computational effort required to reach a minimum solution. Values are chosen such that further increases do not significantly alter the results obtained. For all structures, the region I size used was 0.925 c-axis lattice units (i.e. ≈40 atoms) and region IIa was 2.5 c-axis lattice units (i.e. ≈17,000 atoms). Such large numbers of ions are necessary when modelling complex defects in systems, such as corundum, where the lattice response remains significant over several atomic distances and there is little defect cluster symmetry. Such computational demands can only be provided by modern computer facilities. The simulations were carried out using the CASCADE[45] simulation code.

Table 1
Short-range potential parameters used for host lattices and dopants

Species	Cation radii[48]	A (eV)	ρ (Å)	C (eV Å^6)	Ref.
O^{2-}–O^{2-}	1.40	9547.96	0.2192	32.0	16,49–54
Mg^{2+}–O^{2-}	0.72	1248.38	0.299969	0.0	16
Co^{2+}–O^{2-}	0.745	778.02	0.3301	0.0	54
Fe^{2+}–O^{2-}	0.78	853.5	0.3288	0.0	49
Cd^{2+}–O^{2-}	0.95	951.88	0.34856	13.91	50
Ca^{2+}–O^{2-}	1.00	784.38	0.36356	0.0	50
Sr^{2+}–O^{2-}	1.18	682.17	0.3945	0.0	53
Ba^{2+}–O^{2-}	1.35	905.7	0.3976	0.0	50
Al^{3+}–O^{2-}	0.535	1120.04	0.3125	0.0	–
Cr^{3+}–O^{2-}	0.615	1313.18	0.3165	0.0	–
Ga^{3+}–O^{2-}	0.620	1281.75	0.3175	0.0	–
Fe^{3+}–O^{2-}	0.645	1414.60	0.3128	0.0	50
Sc^{3+}–O^{2-}	0.745	1575.85	0.3211	0.0	50
In^{3+}–O^{2-}	0.800	1495.65	0.3327	4.33	–
Yb^{3+}–O^{2-}	0.868	1649.80	0.3386	16.57	52
Y^{3+}–O^{2-}	0.900	1766.4	0.33849	19.43	50
Sm^{3+}–O^{2-}	0.958	1944.44	0.3414	21.49	52
La^{3+}–O^{2-}	1.032	2088.89	0.3460	23.25	51
Rh^{4+}–O^{2-}	0.600	1204.64	0.3404	0.0	–
Ti^{4+}–O^{2-}	0.605	1210.04	0.3427	0.0	–
Ru^{4+}–O^{2-}	0.620	1215.78	0.3441	0.0	52
Mo^{4+}–O^{2-}	0.650	1223.97	0.347	0.0	52
Sn^{4+}–O^{2-}	0.790	1414.32	0.3479	13.6	52
Pu^{4+}–O^{2-}	0.860	1682.08	0.3542	0.0	–

4. Crystal chemistry

4.1. Crystallography

The host lattices considered are α-Al_2O_3, α-Cr_2O_3 and α-Fe_2O_3. All exhibit the hexagonal corundum structure (space group $R\bar{3}c$) shown in Fig. 1. In this structure cations occupy the 12*c* sites and oxygen ions the 18*e* sites. An important 6*b* interstitial site exists between alternate pairs of cations, seen at the centre of the cation column in Fig. 1. The accuracy to which the potential parameters reproduce the perfect (i.e. defect free) lattice is shown in Table 2.

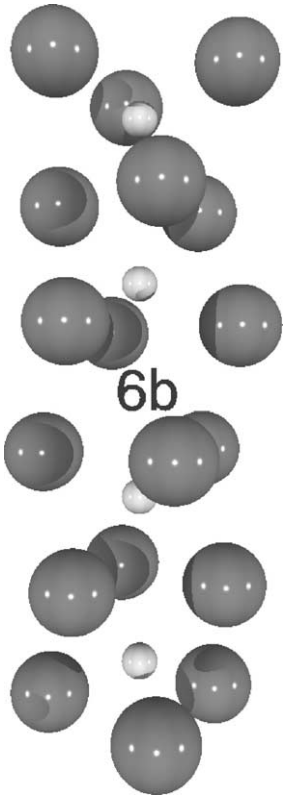

Fig. 1. The corundum structure, large spheres represent oxygen ions on 18*e* sites and small spheres, M^{3+} cations on 12*c* sites. The 6*b* interstitial site is also identified.

Table 2
Host lattice parameters, calculated and experimental[55–57]

Parameter		Al_2O_3	Cr_2O_3	Fe_2O_3
a(Å)	Expt.	4.76050	4.9570	5.0206
	Calc.	4.784	5.038	5.051
c(Å)	Expt.	13.003	13.5923	13.7196
	Calc.	12.9956	113.328	13.345
Vol. (Å^3)	Expt.	255.467	289.242	299.491
	Calc.	255.054	292.992	294.921

4.2. Defect chemistry

4.2.1. Defect process model and equations

Solution of a range of 2+, 3+, and 4+ cation binary oxides into the host corundum lattice was simulated via cation substitution onto a cation 12*c* site. For the 2+ and 4+ cations ionic charge compensation is required and we report the predicted solution energies of possible mechanisms.

For each mechanism we consider the case where defects remain isolated and the case where defects aggregate together to form neutral defect clusters. When predicting the stability of clusters it is useful to consider the binding energy, E^{bin}, which is defined as the difference in energy between the sum of the formation energies of the cluster components when they are spatially isolated, E_{defects}, and the formation energy of the cluster, E_{cluster}.

$$E^{\text{bin}} = \sum E_{\text{cluster}} - E_{\text{defects}} \tag{2}$$

Thus, a negative binding energy indicates that a given cluster is stable. Possible cluster configurations (geometries) were investigated out to the 3rd neighbour. The cooperative relaxation that can occur in defect clusters means that different clusters will introduce different amounts of strain into the lattice. It is important to consider all the possibilities so that the lowest energy (most favourable) can be predicted. This is indicated by the lowest overall binding energy.

Reactions (3)–(11) below detail the important defect processes for these systems where M denotes the host lattice cation (Al^{3+}, Cr^{3+} or Fe^{3+}) and B, C and D denote a dopant ion charge of 2+, 3+ or 4+ respectively. The intrinsic Schottky [reaction (3)], anion Frenkel [reaction (4)] and cation Frenkel [reaction (5)] processes are considered. The isovalent solution process [reaction (9)] is used for 3+ cation incorporation where no charge compensation is required. In the case of 2+ aliovalent cation solution three compensation processes are considered: dopant interstitial [reaction (6)], interstitial [reaction (7)] and vacancy [reaction (8)]. For 4+ aliovalent cation solution two compensation processes are considered: interstitial [reaction (10)] and vacancy [reaction (11)].

- *Intrinsic defect reactions:*

$$2M_M^{\times} + 3O_O^{\times} \rightleftharpoons 2V_M''' + 3V_O^{\bullet\bullet} + M_2O_3 \tag{3}$$

$$O_O^{\times} \rightleftharpoons V_O^{\bullet\bullet} + O_i'' \tag{4}$$

$$M_M^{\times} \rightleftharpoons V_M''' + 2M_i^{\bullet\bullet\bullet} \tag{5}$$

- *Divalent solution reactions:*

$$3BO + 2M_M^{\times} \rightleftharpoons 3B_M^{'} + B_i^{\bullet\bullet} + M_2O_3 \quad (6)$$

$$3BO + 3M_M^{\times} \rightleftharpoons 3B_M^{'} + M_i^{\bullet\bullet\bullet} + M_2O_3 \quad (7)$$

$$2BO + 2M_M^{\times} + O_M^{\times} \rightleftharpoons 2B_M^{'} + V_O^{\bullet\bullet\bullet} + M_2O_3 \quad (8)$$

- *Trivalent solution reaction:*

$$C_2O_3 + 2M_M^{\times} \rightleftharpoons 2C_M^{\times} + M_2O_3 \quad (9)$$

- *Tetravalent solution reactions:*

$$2DO_2 + 2M_M^{\times} \rightleftharpoons 2D_M^{\bullet} + O_i^{''} + M_2O_3 \quad (10)$$

$$2DO_2 + 4M_M^{\times} \rightleftharpoons 3D_M^{\bullet} + V_M^{'''} + 2M_2O_3 \quad (11)$$

4.2.2. Normalisation of defect reaction energies

One stated aim of this study is to predict, for each dopant, the mechanism by which it is incorporated into the lattice, assuming equilibrium (but without, at this stage, recourse to compensation via electronic defects). It is therefore not sufficient to report the intrinsic energies for reactions (3)–(5) or the solution energies for reactions (6)–(11). In each case, the reaction energies must be normalised by a factor derived from a mass action analysis.[15,46]

If we consider first intrinsic Schottky disorder, reaction (3), the corresponding mass action equation is,

$$\left[V_M^{'''}\right]^2\left[V_O^{\bullet\bullet}\right]^3 = e^{\frac{-\Delta H_{sh(8)}}{kT}} \quad (12)$$

where ΔH_{sh} is the predicted energy for reaction (3), k is the Boltzmann constant and T is the temperature. Note that since we are using concentration units in the form of site fractions, terms such as the concentration of oxygen sites, $\left[O_O^{\times}\right]$ are all approximately unity and have therefore not been included for brevity. If the Schottky reaction is dominant then the electroneutrality condition is,

$$3\left[V_M^{'''}\right] = 2\left[V_O^{\bullet\bullet}\right] \quad (13)$$

Substitution of Eq. (13) into Eq. (12) yields,

$$\left[V_M^{'''}\right] = \left(\frac{2}{3}\right)^{\frac{3}{5}} e^{\frac{-\Delta H_{sh}}{5kT}} \quad (14)$$

and,

$$\left[V_O^{\bullet\bullet}\right] = \left(\frac{3}{2}\right)^{\frac{2}{5}} e^{\frac{-\Delta H_{sh}}{5kT}} \quad (15)$$

The Schottky energy is therefore normalised by a factor 5. Similarly anion Frenkel disorder, reaction (4), is normalised by a factor 3 [as is the cation Frenkel reaction (5)].

The analysis for solution reactions (6)–(11) is similar. For example, solution of B^{2+} ions via reaction (8) yields the corresponding mass action equation,

$$\left[B_M^{'}\right]^2\left[V_O^{\bullet\bullet}\right] = e^{\frac{-\Delta H_{sol(8)}}{kT}} \quad (16)$$

where $H_{sol(8)}$ is the predicted energy for reaction (8). If this is the dominant solution mechanism then the electroneutrality condition is,

$$\left[B_M^{'}\right] = 2\left[V_O^{\bullet\bullet}\right] \quad (17)$$

Substitution of Eq. (17) into Eq. (16) yields,

$$\left[B_M^{'}\right] = 2e^{\frac{-\Delta H_{sol(8)}}{3kT}} \quad (18)$$

and,

$$\left[V_O^{\bullet\bullet}\right] = 4^{\frac{-1}{3}} e^{\frac{-\Delta H_{sol(8)}}{3kT}} \quad (19)$$

Therefore the predicted energy for reaction (8) must be normalised by a factor of 3. Similar analysis yields factors of 3 for reaction (6) and 4 for reaction (7).

When considering solution of tetravalent, D^{4+}, ions, reaction (11) yields the corresponding mass action reaction,

$$\left[D_M^{\bullet}\right]^3\left[V_M^{'''}\right] = e^{\frac{-\Delta H_{sol(11)}}{kT}} \quad (20)$$

where $H_{sol(11)}$ is the predicted energy for reaction (11). If this is the dominant solution mechanism then the electroneutrality condition is,

$$\left[D_M^{\bullet}\right] = 3\left[V_M^{'''}\right] \quad (21)$$

Substitution of Eq. (21) into Eq. (20) yields,

$$\left[D_M^{\bullet}\right] = 3^{\frac{1}{4}} e^{\frac{-\Delta H_{sol(11)}}{4kT}} \quad (22)$$

and,

$$\left[V_M^{'''}\right] = 3^{\frac{-3}{4}} e^{\frac{-\Delta H_{sol(11)}}{4kT}} \quad (23)$$

so that reaction (11) is therefore normalised by a factor of 4. Through similar analysis reaction (10) is normalised by a factor of 3.

Finally for isovalent solution of C^{3+} ions, a mass action analysis yields a normalisation factor of 2.

5. Results and discussion

5.1. Intrinsic defect behaviour

The normalised intrinsic defect reaction energies reported in Table 3 suggest that all these disorder reactions are

Table 3
Host lattice intrinsic defect energies normalised per defect

Energy (eV)	Equation	Al_2O_3	Cr_2O_3	Fe_2O_3
Schottky	(3)	5.15	5.59	5.82
Anion Frenkel	(4)	5.54	5.34	5.43
Cation Frenkel	(5)	7.22	7.80	8.07

relatively high energy processes. The Schottky reaction has marginally the lowest energy in α-Al_2O_3 while the anion Frenkel reaction requires marginally the lowest energy in α-Cr_2O_3 and α-Fe_2O_3. Unfortunately, given the small relative difference between these energies, it would be practically impossible to differentiate between reactions experimentally, the same conclusion drawn by El-Aiat and Kröger[22] when studying α-Al_2O_3.

5.2. Extrinsic defect behaviour

5.2.1. General comments

Results of calculations, assuming isolated defects, are presented graphically as normalised solution energy vs. dopant cation radii (see Figs. 2a, 3a and 4a). In these figures the dopant cation size is plotted along the *x*-axis and the solution energies (assuming isolated defects) are plotted along the *y*-axis. Fig. 2 shows results for α-Al_2O_3, Fig. 3 for α-Cr_2O_3 and Fig. 4 for α-Fe_2O_3. As a guide to the eye a quadratic trend-line is fitted to the data for each mechanism. A further 2500 defect calculations were required to explore satisfactorily the effect of clustering in the divalent and tetravalent solution mechanisms. Cluster binding energies are presented in Figs. 2b, 3b and 4b respectively.

Comparing the three systems, solution energies for α-Al_2O_3 are slightly higher and the dopant ion radii dependency is stronger than in α-Cr_2O_3 and α-Fe_2O_3. This is apparent from the higher values and steeper gradients in Fig. 2a, compared to Figs. 3a and 4a. This indicates that if dopants become incorporated in the lattice they will form a second phase more easily if that lattice is α-Al_2O_3. However, this also means that equilibrium dopant concentrations in α-Al_2O_3 will be lower than in α-Cr_2O_3 and α-Fe_2O_3.

We note that generally α-Cr_2O_3 and α-Fe_2O_3 yield very similar results. This can be explained by the very close match between the two lattice volumes (see Table 2). As such, it is difficult to resolve any appreciable variation between the two with respect to solution energies. Of course in low p_{O_2} it is much easier to reduce Fe^{3+} than Cr^{3+} leading to alternative mechanisms in the iron

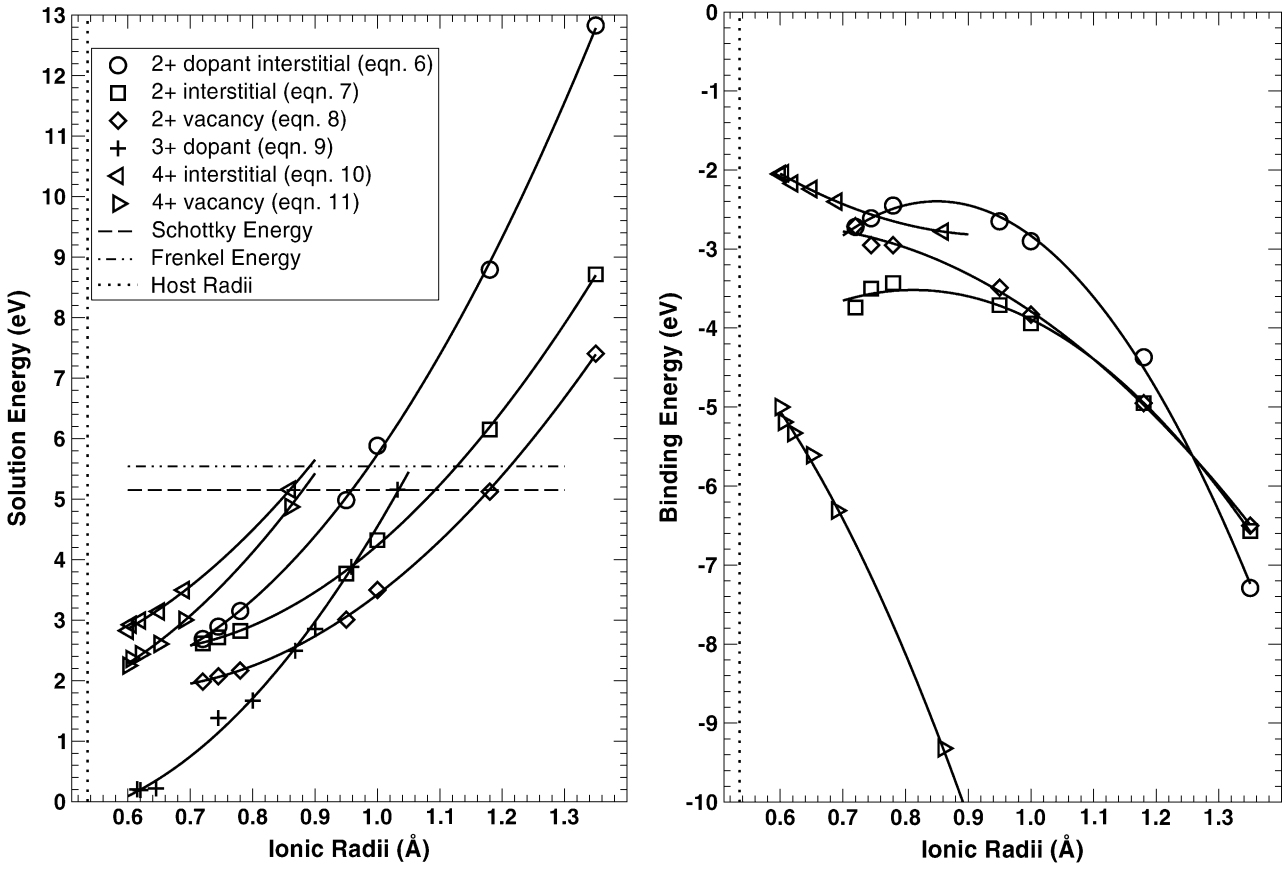

(a) Isolated Solution Energies (b) Cluster Binding Energies

Fig. 2. Al_2O_3 isolated defect solution and cluster binding energetics.

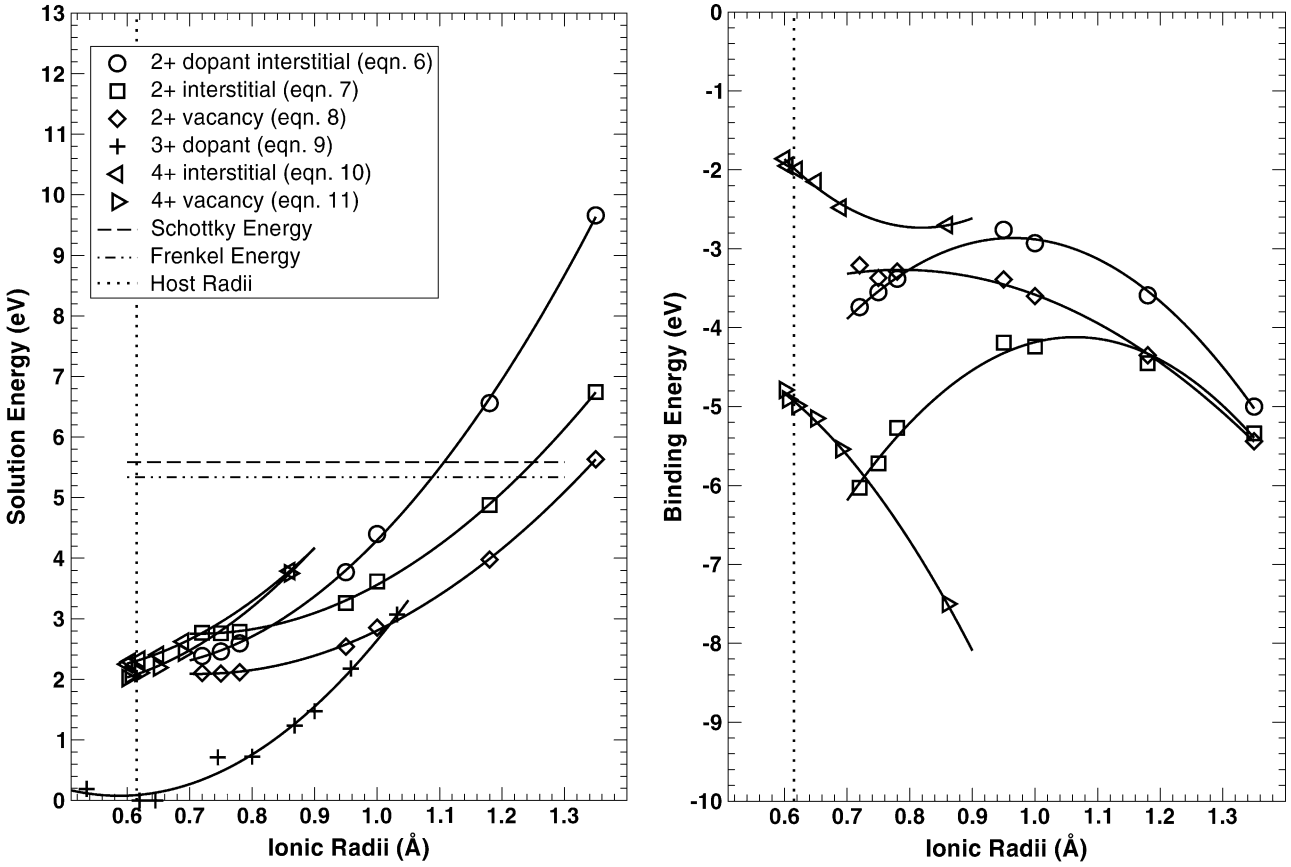

(a) Isolated Solution Energies

(b) Cluster Binding Energies

Fig. 3. Cr_2O_3 isolated defect solution and cluster binding energetics.

system not considered here and as such limits the p_{O_2} range over which this model can be applied. Consequently distinct differences between defect mechanisms can be expected in α-Cr_2O_3 and α-Fe_2O_3 at specific oxygen partial pressures.

5.2.2. Isovalent solution

Isovalent solution will not create charged defects in the lattice [reaction (9)]. Hence, we do not expect these dopant species to increase the concentration of those defects (e.g. vacancies or interstitials) which might aid mass transport through the lattice.[9,10,13,26,35,37] However, the large solution energies for large dopant cations (i.e. Yb^{3+}, Y^{3+}, Sm^{3+} and La^{3+} which range from 2.4 eV to 5 eV in α-Al_2O_3 and 1.2 eV to 3 eV in α-Cr_2O_3 and α-Fe_2O_3) mean that such dopants will not stay in solution but will overwhelmingly form a second phase. The formation of a second phase will obviously lead to complex grain boundary structures. Grain boundaries are likely to provide a lower energy pathway for atomic transport than through the bulk and so are considered deleterious.

Dopant cations with radii close to that of the host lattice cation, exhibit small solution energies. Evidence of a minimum is visible in Figs. 3a and 4a where the host cation radius lies between the minimum and maximum range of 3+ dopants studied. Solution energies increase rapidly as the dopant cation size differs from that of the host. Thus only ions with radii very close to the host lattice radii are likely to exhibit appreciable solubility in these lattices (e.g. Cr^{3+}, Ga^{3+}, Fe^{3+} in α-Al_2O_3; Al^{3+}, Cr^{3+}, Ga^{3+} in α-Fe_2O_3 and; Al^{3+}, Fe^{3+}, Ga^{3+} in α-Cr_2O_3 all of which have solution energies less than 0.5 eV).

5.2.3. Aliovalent substitution

5.2.3.1. Compensation effects. Aliovalent substitution requires intrinsic charge compensating defects [reactions (7), (8), (10) and (11)] or extrinsic charge compensating defects [reaction (6)] to be formed. This may increase the concentration of those species responsible for mediating transport in these host materials. However, there is also the potential to produce defects that will either reduce the mobile species concentration (through the intrinsic defect equilibria) or hinder their transport mechanisms (through defect cluster formation which will be discussed later). Again we must be mindful of the absolute value of the solution energies since large values will result in second phase formation.

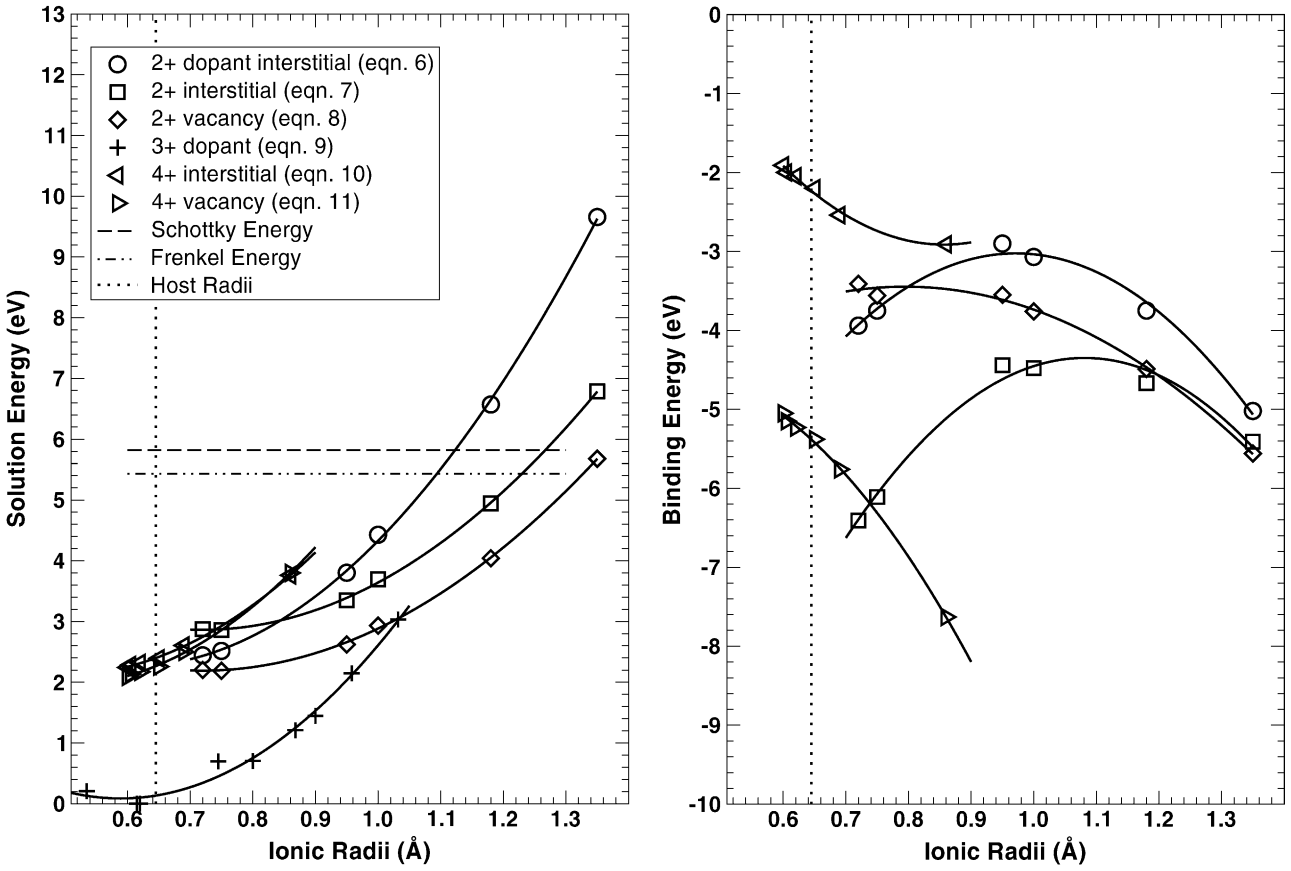

(a) Isolated Solution Energies (b) Cluster Binding Energies

Fig. 4. Fe_2O_3 isolated defect solution and cluster binding energetics.

5.2.3.2. Divalent substitution. For all substitutional divalent cations investigated here [reaction (8)] anion vacancy compensation is the dominant mechanism for the three host oxides (see Figs. 2a–4a). Reaction (6), which assumes compensation via dopant interstitial ions, is close in energy for Mg^{2+} solution (especially in α-Cr_2O_3 and α-Fe_2O_3). However, the differences between the energies for reactions (8) and (6) increase substantially for larger cations.

The solution energy range for divalent ions, assuming isolated defects, is 2.0–7.4 eV, for Al_2O_3, and 2.2–5.6 eV, for α-Cr_2O_3 and α-Fe_2O_3. As a result of these differences we expect that the range of divalent ion radii for which there is any practical solution will be smaller in α-Al_2O_3 than in the other materials. However, in all three host materials only the smallest cations will exhibit significant solution concentration and certainly larger 2+ ions will tend to either form a second phase or will segregate to grain boundaries.

The lowest solution energies are predicted for substitutional ions with smaller radii for all three host lattices as would be expected since the smaller radii cations are closer in size to the host lattice cations. However, the effective size of the substitution site is not exactly the same as that of the host lattice ion that is being replaced. This is because relaxation of the near neighbour oxygen ions is outward, away from the 2+ substitutional ion, since the effective charge of the defect is minus one. This creates a slightly larger substitutional site. Consequently the curves depicting 2+ ion solution as a function of dopant ion radius would exhibit a minimum at a radius larger than that of the host lattice cation.

It is now possible to assess when the extrinsic equilibrium solution of binary oxides, *BO*, results in the formation of greater concentrations of oxygen vacancies, $V_O^{\bullet\bullet}$, than the corresponding lowest energy intrinsic reaction. Since both Schottky and anion Frenkel processes produce oxygen vacancies, and we cannot categorically dismiss one on energetic grounds, both must be compared to the favoured divalent solution mechanism.

We have already derived the equation that describes the equilibrium oxygen vacancy concentration if oxygen vacancies are formed primarily through solution of dopant ions; this is Eq. (19). Conversely if Schottky disorder is dominant (as may be the case in α-Al_2O_3), Eq. (15) will govern oxygen vacancy concentration. However, if anion Frenkel disorder is dominant (as may be the case for α-Cr_2O_3 and α-Fe_2O_3), then,

$$\left[V_O^{\bullet\bullet}\right] = e^{\frac{-\Delta H_{an-fr}}{2kT}} \quad (24)$$

is appropriate where ΔH_{an-fr} is the anion Frenkel reaction energy.

Since the pre-exponential factors in Eqs. (15), (19) and (24) are numerically close we may conclude that the extrinsic reaction will effectively dominate when $\frac{1}{3}\Delta H_{sol(8)} < \frac{1}{5}\Delta H_{sh}$ or $< \frac{1}{2}\Delta H_{an-fr}$. Energies for $\frac{1}{3}\Delta H_{sol(8)}$ are given in Figs. 2a–4a. The normalised Schottky and anion Frenkel energies from Table 3 are also indicated in Figs. 2a–4a by dotted lines parallel to the *x*-axis. Since the majority of points lie below the intrinsic energy lines, extrinsic solution is responsible for oxygen vacancy formation in all three materials except when the dopant 2+ cations are very large (i.e. Sr^{2+} and Ba^{2+} for α-Al_2O_3 and Ba^{2+} in α-Cr_2O_3 and α-Fe_2O_3). Thus, the solution energies for these large cations are sufficiently large and their resulting equilibrium solution concentrations will be so small that they will not alter the intrinsic equilibria.

5.2.3.3. Tetravalent substitution. For tetravalent cation solution in α-Al_2O_3, host cation vacancy compensation [reaction (11)] is the dominant solution mechanism for all dopant ions (see Fig. 2a). This agrees with available experimental evidence for Ti^{4+} solution in α-Al_2O_3.[8,31,32] The solution energies for this solution mechanism, assuming isolated defects, range from 2.2 eV to 4.8 eV. Again we see smaller ions exhibit higher equilibrium solution concentrations (i.e. have lower solution energies) than larger dopant ions. Furthermore, there is a sharp increase in solution energy as the 4+ dopant radius increases. This is because, in the case of a 4+ dopant ion, the effective size of the substitutional site is smaller than the host lattice ion. The smaller site is a consequence of the effective charge of the dopant being positive, such that the near neighbour oxygen ions are drawn slightly inward. Thus, even the smallest 4+ ion is larger than the substitutional site.

For tetravalent ion accommodation in α-Cr_2O_3 and α-Fe_2O_3 the difference between solution energies for reactions (10) and (11) is small. Solution energies for both reactions yield values for α-Cr_2O_3 and α-Fe_2O_3 of between 2.0 eV and 3.8 eV with smaller cations exhibiting the lower solution energies. In fact, reactions (10) and (11) are connected through the Schottky and anion Frenkel reactions,

$$\Delta H_{sol(10)} = \frac{2}{3}\Delta H_{sol(11)} + \Delta H_{an-fr} + \frac{3}{4}\Delta H_{sh} \quad (25)$$

Therefore, whichever reaction is dominant, both the metal vacancy and oxygen interstitial concentrations will increase.

We are now able to predict the tetravalent dopant ions for which solution via reactions (10) and (11) will result in the formation of a greater concentration of metal vacancies than the equivalent intrinsic mass action equilibrium relationship, assuming defects are spatially separated.

The relationship that governs the metal vacancy concentration, assuming solution defects are dominant, is Eq. (23) (which can be modified to yield equivalent equations for oxygen interstitials through Eq. (25). This must be compared to the equivalent lowest energy intrinsic reaction that results in metal vacancy formation. In all three host lattices this is the Schottky process [reaction (3)] and therefore Eq. (14) must be compared to Eq. 23. Again since the pre-exponential factors are numerically close the extrinsic doping reaction will effectively dominate when $\frac{1}{4}\Delta H_{sol(11)} < \frac{1}{5}\Delta H_{sh}$. This inequality can be investigated by comparing energies given in Table 3 and Figs. 2a–4a. Therefore, through the equilibrium solution of any 4+ cation included here, the resulting population of $V_M^{'''}$ (and through reaction 25, $O_i^{''}$) dominates concentrations derived from intrinsic reactions. Since the equilibrium 4+ dopant solution populations are small (i.e. the solution energies are high), there only has to be a small impurity content for the equilibrium solution to be achieved and the intrinsic reaction to be dominated. In α-Cr_2O_3 and α-Fe_2O_3 such an analysis will need to be modified for p_{O_2} and temperature regimes where electronic reactions are important (for α-Al_2O_3 this will not be necessary given the negligible nonstoichiometry that is observed experimentally). For example, electronic defects may well offer a lower energy compensation mechanism for 4+ ion substitution (e.g. via Fe'_{Fe} compensation) so that the $V_M^{'''}$ and $O_i^{''}$ concentrations will not be modified to the same degree. Such reactions will be the focus of subsequent studies.

6. Defect cluster formation

Cluster formation can lead to a substantial reduction in the solution energy although the extent depends on the mechanism and the dopant ion radii. This reduction in energy, the binding energy, is presented graphically in Figs. 2b–4b. The energies are substantial and suggest that strong defect associations will form in these systems at appropriate temperatures. There are two components to the binding energy.[47] Firstly, the coulombic interaction which is a consequence of oppositely charged defects acting to reduce the overall charge disruption in the lattice. Secondly, the lattice relaxation in which the ions move to a more favourable geometry. For example, an anion vacancy close to an over-sized solute cation ion will reduce the overall strain in the lattice.

The extent to which defects will form clusters or remain isolated depends on the magnitude of the binding energy analysed through a mass action relationship.

For example, the defects associated with reaction 8 may form neutral clusters of the type,

$$2B_M^{'} + V_O^{\bullet\bullet} \underset{\text{sol}(8)}{\rightarrow} \left\{2B_M^{'} : V_O^{\bullet\bullet}\right\}^{\times} \tag{26}$$

in which case we can define a mass action equation,

$$\frac{\left[\left\{2B_M^{'} : V_O^{\bullet\bullet}\right\}^{\times}\right]}{\left[B_M^{'}\right]^2\left[V_O^{\bullet\bullet}\right]} = e^{\frac{-\Delta H_{\text{sol}(8)}^{\text{bin}}}{kT}} \tag{27}$$

where $\Delta H_{\text{sol}(8)}^{\text{bin}}$ is the solution energy for reaction (8) when defects form clusters. Since all the binding energies are negative [for reaction (8), and indeed all mechanisms studied here], it is clear that clusters are most stable at low temperatures but tend to break up at high temperatures. This has been studied in detail for Mg^{2+} and Ti^{4+} solution in α-Al_2O_3 previously by Lagerlöf and Grimes[15] who also considered a variety of possible charged defect clusters. Although the details may be quite different for other dopants, the results presented in Figs. 2b–4b suggest that for neutral defect clusters (and by comparison to the results of Lagerlöf and Grimes for charged clusters) similar defect equilibria for cluster formation will occur in all these systems. Since defect cluster formation lowers solution energies it is important to determine if the lowest energy solution mechanism is changed through defect association.

In the case of tetravalent substitution, assuming neutral cluster formation, the two solution mechanisms corresponding to reactions (10) and (11) are, respectively,

$$2DO_2 + 2M_M^{\times} \rightleftharpoons \left\{2D_M^{\bullet} : O_i^{''}\right\}^{\times} + M_2O_3 \tag{28}$$

$$3DO_2 + 4M_M^{\times} \rightleftharpoons \left\{3D_M^{\bullet} : V_i^{'''}\right\}^{\times} + 2M_2O_3 \tag{29}$$

to be able to compare these reactions the equilibrium between them must be stated. This is,

$$\left\{3D_M^{\bullet} : V_M^{'''}\right\}^{\times} + \frac{1}{2}M_2O_3 \rightleftharpoons \frac{3}{2}\left\{2D_M^{\bullet} : O_i^{''}\right\}^{\times} + M_M^{\times} \tag{30}$$

the corresponding mass action relationship is therefore,

$$\frac{\left[\left\{2D_M^{\bullet} : O_i^{''}\right\}^{\times}\right]^{3/2}}{\left[\left\{3D_M^{\bullet} : V_M^{'''}\right\}^{\times}\right]} = e^{\frac{-\Delta H_{30}}{kT}} \tag{31}$$

where ΔH_{30} is the reaction energy when the cluster associated with reaction (11) is transformed into the cluster associated with reaction (10). Since ΔH_{30} is positive, Eq. (31) implies that reaction (29) will dominate reaction (28) at all temperatures. As such, metal vacancy compensation remains energetically favoured for the solution of tetravalent dopant ions. Thus, at lower temperatures, the oxygen interstitial concentration will be further reduced in favour of defect clusters which involve metal vacancies.

Equivalent relationships can be derived between divalent ion solution reactions when clustering occurs. These relationships also show that clustering does not change the preferred mechanism, which therefore remains as vacancy compensation.

For further details of equilibria between clustered, partly clustered (i.e. charged defect clusters) and isolated defect reactions see previous studies of MgO and TiO_2 solution in α-Al_2O_3.[15]

7. Summary

The analysis presented above, while rigorous, is not complete. Currently our discussion and conclusions are only valid under conditions where ionic defects dominate electronic defects in the host materials. Furthermore, we assume equilibrium which, while possible at high temperatures may well not be attainable at low temperatures or for samples that have been quenched from high temperatures. Nevertheless the results (energies) provide useful data for analysis of these materials since they are the driving forces for solution and cluster formation.

The solution mechanisms and corresponding energies for isovalent and aliovalent dopant ions have been predicted. In all cases, energies increase dramatically with increasing dopant ion radius. Fortunately, despite there being a number of possible solution mechanisms, the lowest energy mechanism for divalent ion substitution is compensated by oxygen vacancies for the whole range of dopant ion size (from Mg^{2+} to Ba^{2+}).

In α-Al_2O_3, tetravalent substitution is always compensated by host metal cation vacancies (from Ti^{4+} to Pu^{4+}). Although this remains the case for α-Cr_2O_3 and α-Fe_2O_3, given isolated defects, the oxygen interstitial compensation mechanism is only slightly less favourable. However, if defect clusters form then the cation vacancy mechanism becomes more clearly favoured.

Isovalent ion substitution does not require charge compensation. Nevertheless energies associated with solution of large trivalent ions are high and consequently the equilibrium solution limits of these ions will be very small. Most large isovalent cations will therefore contribute to second phase formation, possibly as grain boundary phases. The same holds true for larger aliovalent dopant ions. So that for all but the smallest aliovalent ions, solution limits will be small.

Despite low solution limits, most aliovalent cations exhibit sufficient concentration that, at equilibrium, their presence in the three corundum lattices will result in concentrations of vacancies which will dominate intrinsic equilibria. Consequently the concentrations of vacancies and interstitial host lattice ions will be dictated entirely by the balance between the total inventories of divalent and tetravalent dopant ions.

Evaluation of the balance will be a difficult task for two reasons; first, the equilibrium concentrations of different aliovalent ions are so different, and second, divalent and tetravalent substitutional ions will themselves form bound defect clusters which will depend strongly on their respective radii.[15] Nevertheless, as shown previously for Mg^{2+} and Ti^{4+} solution, such analysis while complex, is possible.[15]

Some useful general trends are clear. If divalent ions are substituted into a lattice, the oxygen vacancy concentration is driven up. Through the Schottky and Frenkel equilibria this means that metal vacancy and oxygen interstitial concentrations are forced down and metal interstitial concentrations driven up (though the latter will still be small). The opposite situation will evolve through reaction (11) for tetravalent ion solution. These observations are summarised in Table 4.

The results of this study are in general agreement with available experimental data. We have already mentioned that in α-Al_2O_3 the similarity between Schottky and anion Frenkel energies is consistent with the observations of El-Aiat and Kröger.[22] In regard to our prediction that solution of titanium in α-Al_2O_3 is via cation vacancies, we agree with the specific predictions of Perot-Ervas *et al.*[8]

The summary of Table 4 is also consistent with oxygen self diffusion increasing through Mg^{2+} doping and decreasing through Ti^{2+} doping as reported by Lagerlöf *et al.*[28,29] and Haneda *et al.*[30] This is, of course, assuming that oxygen is transported via a vacancy mechanism. In α-Cr_2O_3 we are in broad agreement with previous simulation studies by Lawrence *et al.*[19] We are also in agreement with observation of Hagel and Seybolt[12] that Y^{3+} has a minimal effect on cation diffusion. In contrast we disagree with their observation that Ce^{4+} does not effect cation diffusion. However, given the radius of Ce^{4+},[48] the solution limit of CeO_2 will be small so it should have little effect on cation diffusion even if it does maintain a tetravalent charge (the possibility of forming isovalent Ce^{3+} was mentioned earlier).

Formulation of a model that describes transport through α-Fe_2O_3 will clearly require further work. The present results are consistent with previous suggestions[39,40] that variations in transport properties between samples are due to different impurity contents. That is, the results presented here for α-Fe_2O_3 and indeed all three host oxides suggest that the concentrations of those structural defects (vacancies and lattice ion interstitial species) that mediate transport will depend critically on the balance of impurities. Thus, to some degree, the effectiveness of these oxide films as passive protection against further corrosion will be greatly influenced by impurity content.

Unfortunately the literature is not conclusive as to which defects are important for transport. Nevertheless, it does seem that aluminium vacancies are mobile in α-Al_2O_3.[8–10] In α-Cr_2O_3, chromium is believed to be mobile but the mechanism (via interstitial or vacancy) is disputed.[11,34,35] Again the host cation is believed to be mobile in α-Fe_2O_3, possibly via an interstitial mechanism,[13,14,37,39,40] even though the valance state of the interstitial is not clear with respect to transport.[39,40] It would be possible to use atomistic techniques to make predictions of activation energies for migration and this would certainly be crucial to any continuation of the work presented here.

Finally we should comment on isovalent impurity defects. Of course 3+ cations should not impact on the concentration of defects associated with transport in these materials. However, qualitatively at least, larger 3+ (and indeed 2+ and 4+) cation dopants have high solution energies and will contribute to the formation of grain boundaries and secondary phases. Either structure may be considered deleterious to corrosion protection and thus should be avoided.

Table 4
Relative change in concentration of important defects due to incorporation of dopant ions via predicted dominant reactions

Dominant equation	Dopant		Intrinsic species			
	B'_M	$D^{\bullet}_M$	$M_i^{\bullet\bullet\bullet}$	V'''_M	O''_i	$V^{\bullet\bullet}_O$
(8)	↑	–	↑	↓	↓	↑
(11)	–	↑	↓	↑	↑	↓

Acknowledgements

K.J.W.A. thanks Corus UK Ltd. for financial support under the EPSRC CASE scheme. R.W.G. gratefully acknowledges Los Alamos National Laboratory for support through the Bernd T. Matthias Scholarship. M.R.L. thanks the Worshipful Company of Ironmongers for a UROP summer studentship. The EPSRC provided computing facilities through grant number GR/M94427.

References

1. Hollingsworth, E. H. and Hunsiker, H. Y., 1987, Corrosion of aluminum and aluminun alloys. In *Metals Handbook*, Vol. 13, 9th edn. ASM International, Metals Park, OH pp. 583–609.
2. Davison, R. M., DeBold, T. and Johnson, M. J., 1987, Corrosion of stainless steels. In *Metals Handbook*, Vol. 13, 9th edn. ASM International, Metals Park, OH, pp. 547–565.
3. Bryson, J. H., 1987, Corrosion of carbon steels. In *Metals Handbook*, Vol. 13, 9th edn. ASM International, Metals Park, OH 4407, pp. 509-529.
4. Wright, I. G., 1987. In *Metals Handbook*, Vol. 13, 9th edn. ASM International, Metals Park, OH.
5. Lai, G., 1996, *High temperature Corrosion of Engineering Alloys*, 2nd edn. ASM International, Metals Park, OH, pp. 19–28 (Chapter 3).

6. Himmel, L., Mehl, R. F. and Birchenall, C., Self-diffusion of iron oxides and the Wagner theory of oxidation. *Trans. AIME*, 1953, **197**, 827–843.
7. Shreir, L. L., ed., *Corrosion,* Vol. 1, 2nd edn. Newnes-Butterworths, London, 1976.
8. Petot-Ervas, G., Saadi, B., Petot, C. and Loudjani, M., Transport properties of titanium-doped α-alumina: experimental results. *J. Eur. Ceram. Soc.*, 1996, **17**, 943–950.
9. Jones, T. P., Coble, R. L. and Mogab, C. J., Defect diffusion in single crystal aluminium oxide. *J. Am. Ceram. Soc.*, 1969, **52**, 331–334.
10. Lesage, G., Huntz, A. M. and Petot-Ervas, G., Transport phenomena in undoped and chromium or yttrium doped-alumina. *Radiation Effects*, 1983, **75**, 283–299.
11. Hoshino, K. and Peterson, N. L., Cation self-diffusion in Cr_2O_3. *J. Am. Ceram. Soc.*, 1983, **66**, C202.
12. Hagel, W. C. and Seybolt, A. U., Cation diffusion in Cr_2O_3. *J. Electrochem. Soc.*, 1961, **108**, 1146–1152.
13. Atkinson, A. and Taylor, R. I., Diffusion of ^{55}Fe in Fe_2O_3 single crystals. *J. Phys. Chem. Solids*, 1985, **46**, 469–475.
14. Kofstad, P., *Nonstoichiometry, Diffusion, and Electrical Conductivity in Binary Metal Oxides.* Wiley-Interscience, New York, 1972.
15. Lagerlöf, K. P. D. and Grimes, R. W., The defect chemistry of sapphire α-Al_2O_3). *Acta Matter*, 1998, **46**, 5689–5700.
16. Grimes, R. W., Solution of MgO, CaO, and TiO_2 in α-Al2O3. *J. Am. Ceram. Soc.*, 1994, **77**, 378–384.
17. Catlow, C. R. A., James, R., Mackrodt, W. C. and Stewart, R. F., Defect energetics in α-Al_2O_3 and rutile TiO_3. *Phys. Rev. B*, 1982, **25**, 1006–1026.
18. Dienes, G. J., Welch, D. O., Fischer, C. R., Hatcher, R. D., Lazareth, O. and Samberg, M., Shell-model calculations of some point-defect properties in α-Al_2O_3. *Phys. Rev. B*, 1975, **11**, 3060–3070.
19. Lawrence, P. J., Parker, S. C. and Tasker, P. W., Computer modeling of the defect properties of chromium oxide, Cr_2O_{3-x}. *Advances in Ceramics*, 1987, **23**, 247–256.
20. Catlow, C. R. A., Cornish, J., Hennessy, J. and Mackrodt, W. C., Theoretical calculation of the energies of defect formation and migration in α-Fe_2O_3 and α-Cr_2O_3. *Cryst. Latt. Def. Amorp*, 1987, **15**, 75–80.
21. Berry, F. J., Bohárquez, A. and Moore, E. A., Rationalisation of defect structure of tin- and titanium-doped α-Fe_2O_3 using interatomic potential calculations. *Solid State Comm.*, 1999, **109**, 207–211.
22. El-Aiat, M. M. and Kröger, F. A., Determination of the parameters of native disorder in α-Al_2O_3. *J. Am. Ceram. Soc.*, 1982, **65**, 162–166.
23. Kr̈oger, F. A., Defect related properties of doped alumina. *Solid State Ionics*, 1984, **12**, 189–199.
24. Mohapatra, S. K. and Kr̈ger, F. A., The dominant type of atomic disorder in α-Al_2O_3. *J. Am. Ceram. Soc.*, 1978, **61**, 106–109.
25. Crawley, J. D., Halloran, J. W. and Cooper, A. R., Oxygen tracer diffusion in single-crystal alumina. *J. Am. Ceram. Soc.*, 1991, **74**, 2086–2092.
26. Prot, D. and Monty, C., Self-diffusion in α-Al_2O_3 II. Oxygen diffusion in 'undoped' single crystals. *Phil. Mag. A*, 1996, **73**, 899–917.
27. Reed, D. J. and Wuensch, B. J., Ion-probe measurement of oxygen self-diffusion in single-crystal Al_2O_3. *J. Am. Ceram. Soc.*, 1980, **63**, 88–92.
28. Lagerlöf, K. P. D., Mitchell, T. E. and Heuer, A. H., Lattice diffusion kinetics in undoped and impurity-doped saphire (α-Al_2O_3): a dislocation loop annealing study. *J. Am. Ceram. Soc.*, 1989, **72**, 2159–2171.
29. Lagerlöf, K. P. D., Pletka, B. J., Mitchell, T. E. and Heuer, A. H., Deformation and diffusion in saphire (α-Al_2O_3). *Radiation Effects*, 1983, **74**, 87–107.
30. Haneda, H. and Monty, C., Oxygen self-diffusion in magnesium- or titanium-doped alumina single crystals. *J. Am. Ceram. Soc.*, 1989, **72**, 1153–1157.
31. Mohapatra, S. K. and Kröger, F. A., Defect structure of α-Al2O3 doped with titanium. *J. Am. Ceram. Soc.*, 1977, **60**, 381–387.
32. Rasmussen, J. J. and Kingery, W. K., Effect of dopants on the defect structure of single-crystal aluminium oxide. *J. Am. Ceram. Soc.*, 1970, **53**, 436–440.
33. Mohapatra, S. K. and Kröger, F., Defect structure of α-Al2O3 doped with magnesium. *J. Am. Ceram. Soc.*, 1977, **60**, 141–148.
34. Crawford, J. A. and Vest, R. W., Electrical conductivity of single-crystal Cr_2O_3. *J. Appl. Phys*, 1964, **33**, 2413–2418.
35. Kofstad, P. and Lillerud, K. P., On high temperature oxidation of chromium. *J. Electrochem. Soc.*, 1980, **127**, 2410–2419.
36. Lide, D. R., ed., *CRC Handbook of Chemistry and Physics,* 78th edn. CRC Press, 1997.
37. Chang, R. H. and Wagner, J., Direct-current conductivity and iron tracer diffusion in heamatite at high temperatures. *J. Am. Ceram. Soc.*, 1972, **55**, 211–213.
38. Salmon, O. N., High temperature thermodynamics of the iron oxide system. *J. Phys. Chem.*, 1961, **65**, 550–556.
39. Hoshino, K. and Peterson, N. L., Cation self-diffusion and the isotope effect in Fe_2O_3. *J. Phys. Chem. Solids*, 1985, **46**, 375–382.
40. Hoshino, K. and Peterson, N. L., Cation self diffusion and impurity diffusion in Fe_2O_3. *J. Phys. Chem. Solids*, 1985, **46**, 1247–1254.
41. Born, M. and Mayer, J. E., Zur gittertheorie der ionenkristalle. *Z. Physik*, 1932, **75**, 1–18.
42. Born, M. and Mayer, J. E., The mutual repulsive potential of closed shells. *J. Chem. Phys*, 1934, **2**, 252–259.
43. Dick, B. and Overhauser, A., Theory of the dielectric constants of alkali halide crystals. *Phys. Rev.*, 1958, **112**, 90–103.
44. Mott, N. and Littleton, M., Conduction in polar solids. *Trans. Faraday Soc.*, 1938, **34**, 485–499.
45. Leslie, M., *DL/SCI/TM31T. Technical Report*. SERC Daresbury Laboratory, 1982.
46. Kingery, W. D., Bowen, H. K. and Uhlmann, D. R., *Introduction to Ceramics,* 2nd edn. John Wiley, New York, 1976.
47. Zacate, M. O., Minervini, L., Bradfield, D. J., Grimes, R. W. and Sickafus, K., Defect cluster formation in M_2O_3-doped cubic ZrO_2. *Solid State Ionics*, 2000, **128**, 243–254.
48. Shannon, R. D., Revised effective ionic radii in halides and chalco-genides. *Acta. Cryst. A*, 1976, **32**, 751–767.
49. Minervini, L. and Grimes, R. W., Defect clustering in wustite. *J. Phys. Chem Solids*, 1999, **60**, 235–245.
50. Grimes, R. W., Busker, G., McCoy, M. A., Chroneos, A. and Kilner, J. A., The effect of ion size on solution mechanism and defect cluster geometry. *Ber. Bunsenges. Phys. Chem.*, 1997, **101**, 1204–1210.
51. Minervini, L., Zacate, M. O. and Grimes, R. W., Defect cluster formation in M_2O_2-doped CeO_2. *Solid State Ionics*, 1999, **116**, 339–349.
52. Minervini, L., Grimes, R. W. and Sickafus, K. E., Disorder in pyrochlore oxides. *J. Am. Ceram. Soc.*, 2000, **83**, 1873–1878.
53. McCoy, M. A., Grimes, R. W. and Lee, W. E., Phase stability and interfacial structures in the SrO–$SrTiO_3$ system. *Phil. Mag. A*, 1997, **75**, 833–846.
54. Chen, S. P., Yan, M., Grimes, R. W. and Vyas, S., Energies and configuration of defects in Ga, Cr, and In-doped CoO. *Ceramic Trans*, 1997, **69**, 129–134.
55. Thompson, P., Coxand, D. E. and Hastings, J. B., Rietveld refinement of Debeye-Scherrer synchrotron X-ray data from Al_2O_3. *Journal of Applied Crystallography*, 1987, **20**, 79–83.
56. Sawada, H., Residual electron density study of chromium sesquioxide by crystal structure and scattering factor refinement. *Mat. Res. Bull*, 1994, **27**, 239–245.
57. Yu, S. C., Lee, J. S., Tung, S. F. and Lan, C. L., Synthesis and structural features of a flux-grown hematite. *J. Geological Soc. China*, 1999, **42**, 349–358.